Passive Microwave Biosensor for Real-Time Monitoring of Subsurface Bacterial Growth

Mandeep Chhajer Jain, *Student Member, IEEE*, Anupama Vijaya Nadaraja, Sevda Mohammadi, *Student Member, IEEE*, Bianca Marjan Vizcaino, and Mohammad Hossein Zarifi, *Senior Member, IEEE*

***Abstract*—A real-time and label-free microstrip sensor capable of detecting and monitoring subsurface growth of Escherichia coli (*E. coli*) on solid growth media such as Luria-Bertani (LB) agar is presented. The microwave ring resonator was designed to operate at 1.76 GHz to detect variations in the dielectric properties such as permittivity and loss tangent to monitor bacterial growth. The sensor demonstrated high efficiency in monitoring subsurface dynamics of *E. coli* growth between two layers of LB agar. The resonant amplitude variations (Δ Amplitude (dB)) were recorded for different volumes of *E. coli* (3 μL and 9 μL) and compared to control without *E. coli* for 36 hours. The control showed a maximum amplitude variation of 0.037 dB, which was selected as a threshold to distinguish between the presence and absence of *E. coli* growth. The measured results by sensors were further supported by microscopic images. It is worth noticing that the amplitude variations fit well with the Gompertz growth model. The rate of amplitude change correlating bacteria growth rate was calculated as 0.08 and 0.13 dB/hr. for 3 μL and 9 μL of *E. coli*, respectively. This work is a proof of concept to demonstrate the capability of microwave sensors to detect and monitor subsurface bacterial growth.**

***Index Terms*—Microwave resonator, subsurface growth, gompertz growth model, growth rate.**

I. Introduction

INFECTIOUS diseases caused by virus/bacteria pose a serious challenge to public health and the global economy [1]–[5]. This is evident from previous clinical reports; for example, approximately 75000 cases of sepsis, an immunological response to infection, is reported in the United States annually [5]. Another infectious disease, periodontitis, is reported to affect 20–50% of the population on a global scale [6]. A recent addition to this is the Covid-19 pandemic, which rapidly spread across the world with 509164 cases and 23335 deaths globally as of March 27, 2020, as reported by the World Health Organization (WHO) [1], [4], [7].

Biofilm bacteria are of great concern, especially in spreading infections via medical devices thereby limiting the reusability of medical devices [8]–[12]. According to the U.S Department of Health and Human Services, approximately 1 in every 24 patients in the USA have an infection related to hospital care and healthcare due to contaminated medical devices harboring biofilm formation [8], [13]. Biofilm formation progresses by transitioning of 2-Dimensional bacterial growth to 3-Dimensional growth [14]. To briefly explain, within a biofilm micro colony several forces act on the bacteria: i) repulsive forces between the bacteria, ii) frictional force between the bacteria, and iii) elastic forces of the surrounding media. In the absence of these forces, bacterial colony transition from 2D to 3D is confined to the surface of the medium. On the other hand, these forces cause bacteria to penetrate the medium rather than growing just on the surface, and this penetration often leads to deep tissue injury [10], [15], [16]. Henceforth, early detection of biofilm-forming pathogens in the tissues is critical in preventing life-threatening infections. This is significant due to a rapid increase in infections which is predicted to increase to as high as 171 million by 2030 with an economy loss of $4 in productivity for every dollar spent on healthcare [17]. This demands innovative techniques for rapid pathogen diagnosis.

The current technologies to detect pathogens rely on either conventional culture-based assays or molecular methods such as polymerase chain reaction (PCR) and enzyme-linked immunosorbent assays (ELISA). However, these are often limited by longer detection time, as in the case of culture-based assays, or require extensive sample preparation and expensive instrumentations in the case of molecular tools [18]–[20]. To overcome these limitations, researchers have developed biosensors for rapid detection and monitoring of microbial growth that can be used in pathogenic detection [21]–[26]. Of these techniques, optical and electrochemical biosensors were widely used owing to their real-time, automated, and label-free detection. However, optical biosensors suffer from high cost and quick degradation of reagents, whereas electrochemical biosensors suffer from a low selectivity and limit of detection (LoD) [26]. Bio-FET is another class of biosensors that are gaining popularity due to their label-free, ultra-high sensitivity, scalability, low cost of fabrication, and minimum power consumption [26]–[29].

Manuscript received September 19, 2020; revised November 25, 2020 and December 29, 2020; accepted January 22, 2021. Date of publication January 29, 2021; date of current version March 30, 2021. This work was supported in part by the Natural Sciences and Engineering Research Council of Canada, through a Discovery Grant Canada Foundation for Innovation (CFI) program, and CMC Microsystems Software and Equipment, and in part by the Department of National Defense- Innovation for Defense Excellence and Security (DND-IDEaS) Program. *(Corresponding author: Mohammad Hossein Zarifi.)*

The authors are with Okanagan Microelectronics and Gigahertz Laboratory (OMEGA Lab), School of Engineering, The University of British Columbia, Okanagan Campus, Kelowna, BC V1V 1V7, Canada (e-mail: mandeepchajerjain@gmail.com; anupilla@gmail.com; sevda.mohammadi@ubc.ca; vizcainobianca27@gmail.com; mohammad.zarifi@ubc.ca).

Color versions of one or more figures in this article are available at https://doi.org/10.1109/TBCAS.2021.3055227.

Digital Object Identifier 10.1109/TBCAS.2021.3055227

Although the benefits of bio-FET make it a promising candidate for the detection and monitoring of bacteria, these sensors cannot be used in contactless applications. Recently, microwave sensors have emerged as a potential detection method for various applications including ice detection [30], wireless permittivity sensing [31]–[36], dielectric spectroscopy [37]–[40], monitoring cancer [41], [42], detection of glucose and electrolyte level in aqueous solution [43]–[47], monitoring water quality [48], and classification and monitoring of bacteria in liquid medium [49]–[55], owing to their numerous advantages such as low cost, real-time, label-free, and non-contact monitoring capabilities. Interestingly, bacterial growth monitoring using microwave sensors is gaining more attention in recent years. Bacterial growth and its correlation with dielectric variations in the surrounding environment has been successfully demonstrated [56]–[59]. In a study using microwave microfluidic biosensor, Narang *et al.* [54], was able to monitor bacterial growth in liquid growth medium and reported a sensitivity of 3.4 MHz/log (OD_{600}). In another study, various concentrations of *E. coli* in liquid culture media were measured using a microwave biosensor operating between 1–3 GHz and was able to achieve a detection limit of 10^3 CFU/ml [55].

Detecting bacterial growth in a solid medium is a real challenge to microbiologists due to the complex nature of solid agar, and the limitations of conventional plating techniques. Recently, microwave sensors were successful in demonstrating bacterial growth detection on solid agar [60], [61]. This offers an avenue to understand bacterial responses to various environmental factors in solid matrix even during the early stages of bacterial growth. Previously, Mohammadi *et al*. [60], monitored bacterial growth on LB agar using a differential microwave resonator operating at 1.95 GHz and 2.11 GHz. The differential resonator was employed to cancel out the effect of external ambient factors such as temperature and humidity on the response of the sensor. Bacterial growth monitoring was achieved by measuring the impact on the response of the resonator due to dielectric variations in the growth medium caused by bacteria metabolism [56]–[59], [62]–[65]. Their work successfully demonstrated the capability of a microstrip resonator to monitor bacteria growth on the surface of solid agar.

With the ever-increasing threat of bacteria biofilms on the health and wellness of human beings, various studies have been performed to understand the growth mechanism of biofilms [8]–[12]. Previous studies on the growth of microorganisms have shown that a crucial stage in the subsurface bacterial growth involves the transition of lateral or 2-Dimensional growth into 3-Dimensional growth into the medium due to mechanical forces acting on the bacteria [14]. Various studies have investigated the effects of mechanical forces on the planar to the bulk transition of bacteria sandwiched between two mediums [10], [16].

Through this work, the capability of the microwave sensor to monitor subsurface bacterial growth was explored. To the best of our knowledge, this is a maiden attempt in this direction. A one-port microstrip line resonator was employed to monitor the bacteria growth. A critically coupled reflection resonator sensor was employed due to its extensive application in the accurate determination of variations in the dielectric properties of highly dissipative (lossy) and conductive environment [66], [67]. The experiment was carried out at two different initial volumes of *E. coli* i.e., 3 μL and 9 μL sandwiched between two layers of solid LB agar using a microwave resonator owing to their robustness, low fabrication cost, contactless and label-free properties. The changes in the characteristics of the medium due to the lateral and subsurface growth of the bacteria are studied by measuring the variation in the resonant amplitude of the microstrip resonator at two different volumes of bacteria.

II. Sensor Design and Simulation

A. Microwave Resonator Design and Simulation

A one-port microwave ring resonator was designed and implemented as the core of the sensing platform. A single port microstrip ring resonator was chosen due to its ability to detect variations in the dielectric properties of dissipative materials. Among various types of resonators available, frequency variation resonators consisting of a single split-ring resonator coupled to a transmission line was selected. Frequency variation resonators are compact and are operated in steady environmental conditions [32], [68]. Therefore, as an incubator was employed to monitor bacterial growth, a single split ring frequency variation resonator was chosen as opposed to a differential resonator. The resonator was monitoring the dielectric property's variations, mainly permittivity and loss tangent, on its sensitive region, where the interactions between the electromagnetic field and the material under test happened. The test material affected the electrical characteristics of the ring resonator such as resonant frequency, resonant amplitude, and quality factor, and was monitored by a vector network analyzer (VNA).

The operation principle of the designed sensor was investigated by implementing a structural model in High-Frequency Structure Simulator (HFSS) and performing finite element method simulations. Furthermore, a lumped circuit model was implemented in Advanced Design System 2020 (ADS) simulator, to justify the sensor's behaviour via the circuit model. Fig. 1(a) presents the implemented structure and the dimensions of the microstrip lines. An alignment arch was incorporated in the actual design to align the resonator with the sample petri dish. The physical size of the resonator was chosen to achieve a resonant frequency of 1.76 GHz, which lies in the L- Band of the microwave spectrum. (1) presents the relation between the resonant frequency and the length of the resonator.

$$l = \frac{c}{2 * f_{res} * \sqrt{\varepsilon_r}} \tag{1}$$

Where f_{res} the resonant frequency, c is the speed of light in vacuum, and ε_r is the relative permittivity of the carrying substrate. Based on (1), the length of the split ring was calculated as 57.5 mm. To increase the sensing area of the resonator to monitor the entire region of the spotted *E. coli*, the length of the resonator gap was chosen as 5 mm. The total length of the resonator was adjusted to accommodate the increase in the sensing area to obtain the desired resonant frequency. The width of the microstrip lines, the coupling gap, and the resonant gap was optimized to achieve the minimum notch amplitude in the

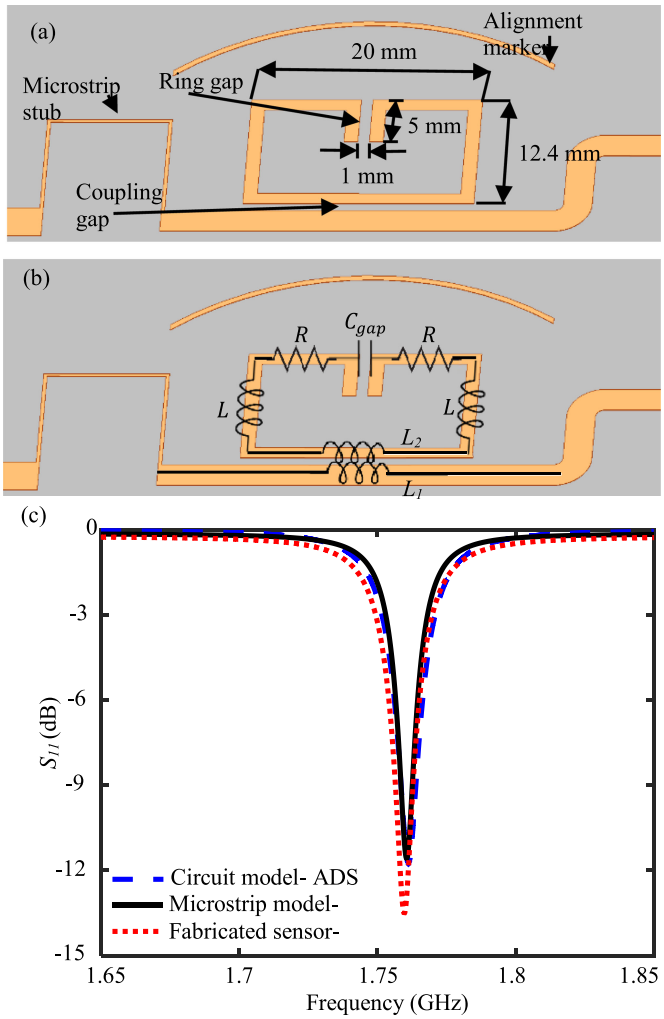

Fig. 1. (a) Microstrip ring resonator structure modelled in HFSS. (b) Microstrip ring resonator structure with its equivalent lumped parameter model. The values for inductance, capacitance and resistance are L = 2.5 nH, $L_1 = 1.5$ nH, $L_2 = 0.5$ nH, $C_{gap} = 1.63$ pF and R = 0.12 Ω respectively. (c) Simulated and measured results of the designed sensor.

S_{11} profile and optimum sensitivity in the sensor's response. The feedline was matched to the characteristic impedance of 50 Ω (port impedance of a standard VNA) using LineCalc (Advanced Design System 2020) to achieve maximum power transmission from the microwave source to the sensor. A high impedance quarter wavelength microstrip stub terminated with a ground plane was added to the resonator model to discharge any static charge accumulated due to the presence of weak capacitance between the feed line and the sample under test.

The high impedance microstrip stub was realized by decreasing the width of the microstrip stub to 0.3 mm, as evident from (2).

$$z = \frac{87}{\sqrt{\varepsilon_r + 1.41}} \ln\left(\frac{5.98 \times h}{0.8 \times w + t}\right) \quad (2)$$

Where z is the characteristic impedance of the microstrip line, h is the height of the substrate, ε_r is the relative permittivity of the carrying substrate, w is the width of the microstrip line, and t is the thickness of the copper cladding.

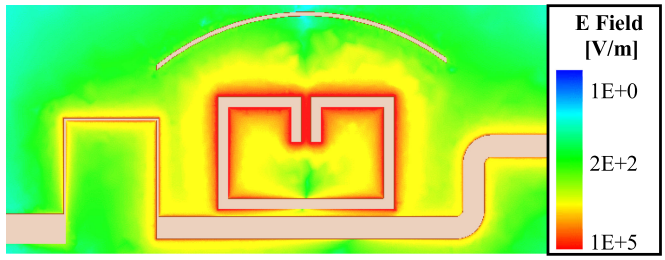

Fig. 2. Electric field distribution on the resonator model simulated at 1.76 GHz using HFSS.

The stub acts as an open circuit to the electromagnetic signals and transfers any static charge accumulated on the sensor's surface to the ground.

To justify the behaviour of the microstrip resonator, a lumped-element model was proposed as shown in Fig. 1(b). The resonator was modelled using a series RLC resonator resonating at a frequency f_{res}. The series RLC circuit was at resonance when the average stored magnetic energy in the circuit equals to the average stored electrical energy, thereby leading to an input impedance that is purely real [69]. In this work, the lumped-element model of the resonator was designed and simulated in Advanced Design Systems (ADS) 2020 by Keysight Technologies. Based on the resonant frequency, the inductance (L) and capacitance (C_{gap}) of the network was calculated using (3).

$$L * \ C_{gap} = (2\pi f_{res})^{-2} \quad (3)$$

The series resistance (R Ω) of the network was kept to a minimum, and the feedline and the split ring resonator were critically coupled to improve the quality factor of the S_{11} notch. The inductance (L nH) and capacitance ($C_{gap}\, pF$) was calculated using (3) and found to be 5 nH and 1.63 pF, respectively. The Coupling capacitance ($C_c = 0.0001$ pF) was negligible and had no impact on the result. Thus, by maintaining a low coupling capacitance ($C_c\, pF$) and minimizing series resistance (R Ω), a desired S_{11} response at the desired resonant frequency was obtained by modelling the sensor structure. Fig. 1(c) compares the simulation results of the implemented sensor structure in HFSS and the simulated associated circuit model in ADS against the measured results of the fabricated sensor. According to the simulated results, the S_{11} response of the Lumped-element model is in good agreement with the simulated bare result of HFSS.

To investigate the sensitive regions of the designed sensor to the dielectric property's variation in the sensor's near environment, the electric field was investigated at the resonant frequency in HFSS simulation. The sensitive region on the microstrip resonator is the region with maximum concentration of electric field. The electric field interacts with the molecules of the sample under test (SUT). This interaction alters the resonant profile of the resonator through which SUT is detected and characterized. According to the simulation results, the resonant gap is highly concentrated with the electric field and was selected to monitor bacterial growth. From Fig. 2, it can also be observed that the

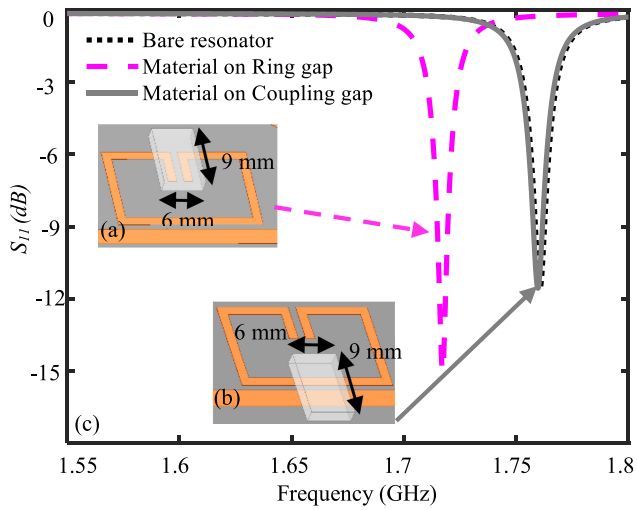

Fig. 3. Test sample on the (a) ring gap, and (b) coupling gap. (c) HFSS simulation results comparing the response of the resonator when the test sample lies on the ring gap and coupling gap.

alignment marks and the microstrip stub had no impact on the electric field distribution and the response of the resonator. However, to validate the sensing region of the sensor, an investigation in HFSS has been performed by placing test material at two different locations as shown in Fig. 3(a) and Fig. 3(b). The test material had a permittivity of 2.2, loss tangent of 0.0009, and a dimension of $6 \times 9 \times 1.79$ mm. The parameters of the test material such as the dimension, orientation, and distance from the sensor were kept constant.

According to the simulated results shown in Fig. 3(c), a variation of 64 MHz and -2.79 dB was observed while the test sample was placed over the ring gap, which is larger than the shift of 1 MHz and -0.01 dB observed at the coupling gap due to the test sample shown in Fig. 3(c). Thus, the ring gap was found to be responsive to the presence of the test material as compared to the coupling gap and was thus chosen. Since the ring gap demonstrated high sensitivity to the presence of a test sample, the sensor's response to variations in permittivity and loss tangent of test material at the ring gap was simulated, and its response was studied. The attributes of the test material such as orientation, dimension, and the gap between the test material and the microstrip structure were constant.

The effect of permittivity and loss-tangent variation in the resonant gap was investigated and studied employing a test material with a size of $6 \times 9 \times 1.79$ mm and changing the permittivity and loss tangent in the range of 1.5 to 3.0 and 0.0001 to 0.0009, respectively. Fig. 4 presents the results for the simulations in HFSS. According to these results, the resonant amplitude of the sensor decreased as the loss tangent of the test sample increased from 0.0001 to 0.0009 in steps of 0.0002 with constant permittivity of 2.2 as shown in Fig. 4(a) and (b) while the resonant frequency remains unchanged. However, a decrease in the resonant frequency was observed as the permittivity of the test sample increased from 1.5 to 3 in steps of 0.5 with a constant loss tangent of 0.0009. The resonant amplitude also exhibited a decrease from -15.4 dB to -16.8 dB as the permittivity of the test sample increased from 1.5 to 3 in steps of 0.5 with a constant loss tangent of 0.0009 as shown in Fig. 4(c) and (d). The results from Fig. 4 demonstrate, if the change is observed mainly in the resonant amplitude with a relative constant resonant frequency, which can be attributed mainly to the loss tangent variation in the medium and not the permittivity. In bacterial growth experiments, it is expected to observe significant conductivity variation in the culture media than the permittivity [70], therefore resonant amplitude was monitored as the main sensing factor to achieve the experimental results.

III. Material And Methods

A. Bacterial Growth Media and Culturing

Soft LB agar was used as culture media for growing *E. coli*. The composition of media is as follows: 1 gram of LB broth and 0.5 gram of agar was weighed and dissolved in 50 mL of RO water. The growth media was then sterilized by autoclaving at 121 °C for 15 minutes in an autoclave. Three ml of this sterile media was then added to a petri dish to prepare LB agar media of 1 mm thickness.

Three μl of *E. coli* from stock culture (OD600 = 1.5) was spotted at a designated position in the agar plate. The spot was covered with an 18×18 mm coverslip, which was evenly coated with 8 ml of soft agar as shown in Fig. 5(a) and (b). Special attention was given to confirm *E. coli* was positioned between the two layers of agar. The petri dish was then sealed with parafilm to avoid contamination of the inoculated sample and to isolate the bacterial growth environment from external humidity variations.

B. Microwave Sensor Fabrication

The designed microstrip structure was fabricated on a standard substrate (Rogers 5880) with a permittivity of 2.2 and loss tangent of 0.0009, as shown in Fig. 6(a). The thickness of the substrate was 0.79 mm, and the thickness of the copper layer was 35 μm. The fabricated sensor was contained in a Styrofoam enclosure for thermal insulation and to minimize the influence of temperature and humidity variation in its near environment, as shown in Fig 6(b). A temperature sensor was employed to monitor the temperature on the sensor substrate, very close to the agar media. The scattering parameter response from the sensor was measured using a vector network analyzer, ZNB20 from Rohde and Schwarz.

The network analyzer was calibrated before each measurement with the calibration frequency range of 1.55 GHz to 1.8 GHz and IF bandwidth of 300 Hz. 6401 was set as the number of the points before the measurements. The output power of the VNA was set to 0 dB i.e., 1 mW. As the input power was sufficiently low, it had no impact on bacterial growth [71]. Furthermore, the intensity of the power radiated from the sensitive region of the resonator was measured using a handheld RF spectrum analyzer and was found to be below -70 dB, which ascertained that the power radiated at resonance had minimal to no impact on the operation of nearby electronic devices. Additionally, any residual cross-coupling between the sensor and readout circuit was weakened by maintaining considerable distance between the readout circuit and the sensor. LabVIEW

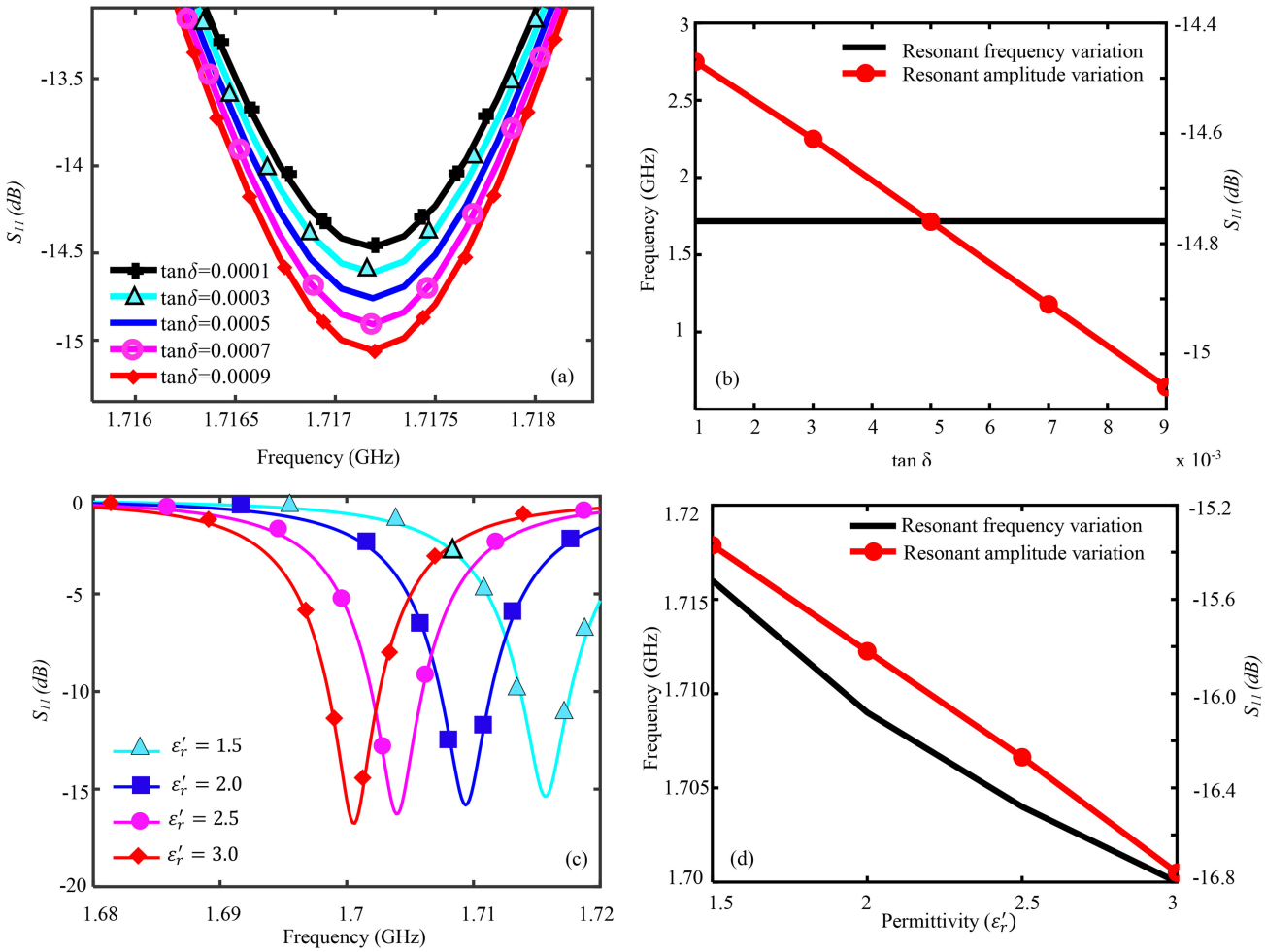

Fig. 4. Effect on the resonant profile (resonant amplitude and frequency) due to variation of loss tangent (a) and (b), and permittivity (c) and (d) of a material under test on the ring gap.

was used to automatically record the S_{11} response every 2 minutes. All the experiment was repeated five-times to demonstrate the repeatability and reproducibility of the experimental results. A digital microscope from Celestron was utilized to capture time-lapse images during the growth process.

IV. Experimental Results and Discussion

Prior to performing the experiments on bacterial growth monitoring, the performance of the sensor was confirmed via standard measurements using standard samples. The S_{11} response of the fabricated sensor in the absence of any test material was measured using the vector network analyser, as shown in Fig. 7.

The resonant frequency of the fabricated sensor in the absence of any test sample was measured as 1.76 GHz with a resonant amplitude of -13.52 dB. The performance of the fabricated sensor was validated by measuring the response of the sensor in the presence of a test sample cut from a standard Rogers 5880 substrate from Rogers Corporation [72]. The test sample had a permittivity of 2.2 and a loss tangent of 0.0009 with structural dimensions of $6 \times 9 \times 1.79$ mm. To validate the sensitive region of the resonator, determined during the field simulation of the proposed sensor, the test sample was placed on the ring gap and the coupling gap as shown in Fig. 7. As evident from the measured result shown in Fig. 7, a 50 MHz and -2.5 dB shift in the resonant profile of the sensor from its initial position was noted when the test material was placed on the resonant or the ring gap whereas a shift of 1 MHz from its initial position was observed when the test material was placed on the coupling gap. Thus, the ring gap was found to be responsive to the presence of the test sample, and the dielectric loading of the coupling gap had no impact on the response of the resonator and was in good agreement with the simulated results.

To characterize the effective dielectric properties of solid LB agar encased in a petri dish, the N1501A dielectric probe kit (Keysight Technologies) was used. The dielectric probe measurement was used qualitatively to determine the resonant frequency of the designed sensor. The dielectric probe was calibrated using standard RO Water at room temperature from 1 GHz to 3 GHz. To measure the dielectric properties, the petri dish with soft agar was positioned in close contact with the dielectric probe, as shown in Fig. 8(a). The agar was properly solidified and sealed within the petri dish using paraffin wax strips. This was done to prevent change in the humidity in

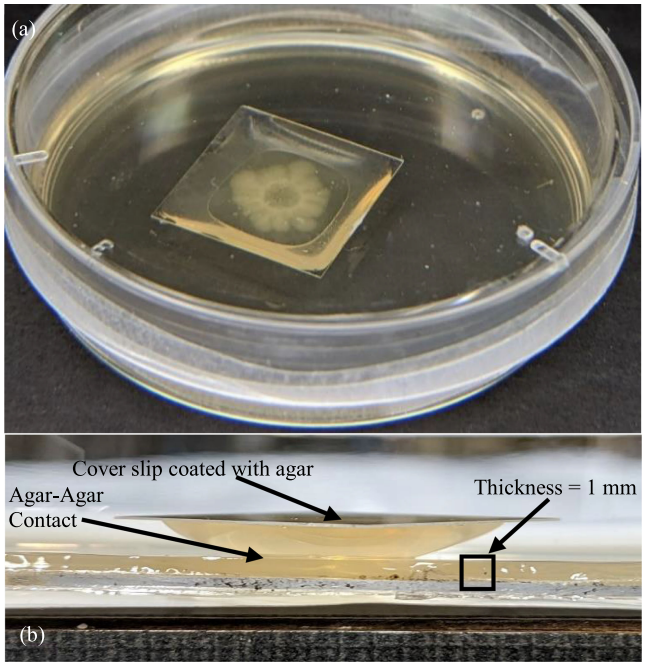

Fig. 5. (a) Top view of the solid agar plate with E. coli enclosed between two layers of agar. (b) Cross section of the agar-agar interface indicating the agar-agar interface between two layers of agar.

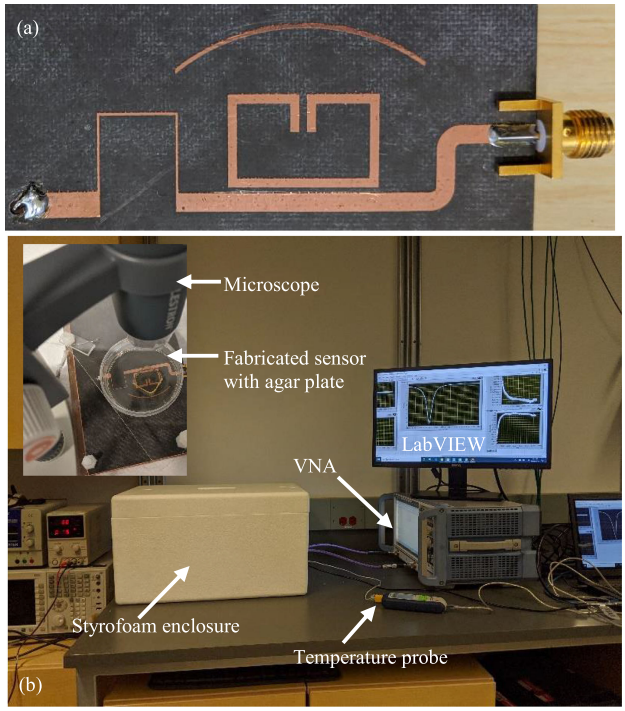

Fig. 6. (a) Fabricated sensor. (b) Experiment setup comprising of VNA, Styrofoam apparatus containing, sensor, inoculated sample and microscope, and temperature sensor.

the petri dish. An average of 16 consecutive measurements was taken to avoid errors. Based on the measured effective permittivity and effective loss tangent presented in Fig. 8(b), a low effective loss tangent in the lower end of the L-band (1 GHz to 2 GHz) of the microwave spectrum was observed. Therefore, to shrink the size of the resonator and maintain an effective low loss characteristic of the sample enclosed in the petri dish, the resonant frequency was chosen as 1.76 GHz.

To test the efficacy of the sensor to detect subsurface bacterial growth, a preliminary test was conducted with and without the presence of a coverslip to allow bacterial growth penetration to soft agar medium. This test was conducted as follows: two Petri dishes with 1 mm thick agar each spotted with 3 μL of *E. coli.* In one plate (control) there was no coverslip, but in the second petri dish (test) *E. coli* was covered with a coverslip coated with a layer of agar (8 ml) to monitor subsurface growth. Both plates were incubated for 48 hours. The *E. coli* grown on the control plate exhibited three-dimensional growth on the surface of the agar. However, in the test, initially, a lateral surface growth was observed followed by a penetrated growth into the subsurface agar medium (Fig. 9).

In the further experiment, *E. coli* was inoculated to a position between two layers of agar and was placed on the microstrip sensor such that the position of inoculated *E. coli* was aligned directly above the sensitive region on the resonator. The S_{11} response of the sensor was measured using VNA and recorded using LabVIEW. The initial measured resonant amplitude for various volumes of *E. coli* was subtracted from their corresponding measured dataset and plotted in Fig. 10(a). The measured data pertained to the initial 90 minutes of the experiment was excluded accounting time for stabilization of the apparatus. For

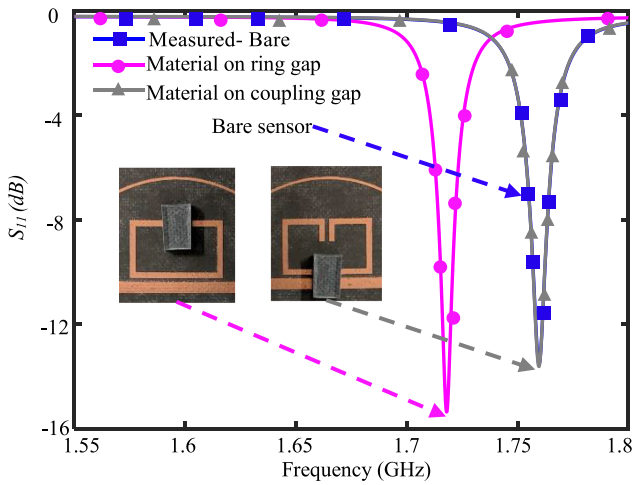

Fig. 7. Measured results with test sample on the ring gap and coupling gap.

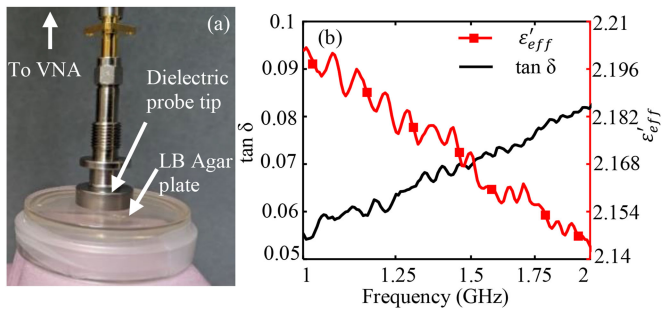

Fig. 8. The experiment setup consisting of N1501A dielectric probe placed in proximity of the solid LB agar plate for dielectric property measurement. (b) The measured dielectric properties of solid LB agar.

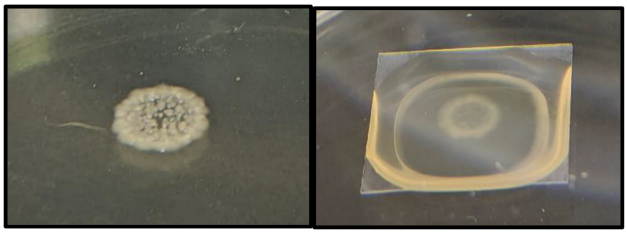

Fig. 9. Three-dimensional growth of *E. coli* on LB-agar with and without the presence of a coverslip coated with LB-agar.

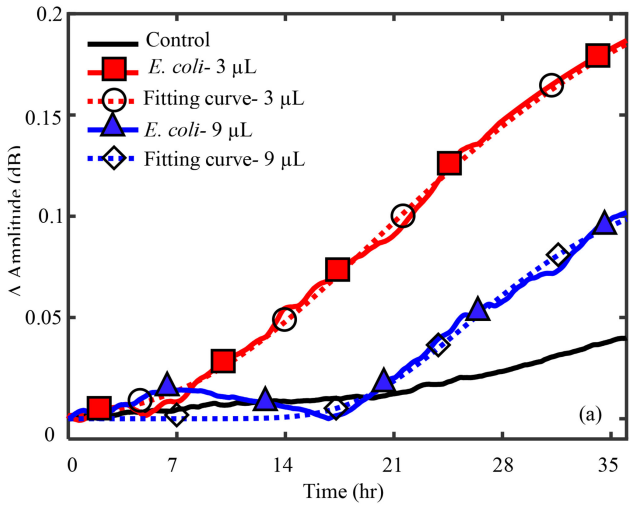

Fig. 10. Measured Δ Amplitude (dB) for 3 μL and 9 μL of *E. coli* on L.B agar and the fitted Gompertz model curve at constant time intervals for 3 μL and 9 μL of *E. coli.*

the total experimental duration of 36 hours, the three times of the measured standard deviation: 0.18, and 0.09 dB, for 3, and 9 μL of *E. coli*, respectively, were well below the reported values for the measured subsurface growth.

Variation in the resonant amplitude can be attributed to change in the conductivity or loss tangent of the growth media due to bacteria growth. However, resonant frequency variation can be associated with a change in the permittivity of the material, which can be associated with a change in the temperature and other physical conditions surrounding the growth media. Since, the variation in the resonant frequency for control, i.e., no bacteria, 3 μL, and 9 μL of *E. coli* was negligible, it was inferred that the fluctuations in the environmental parameters were negligible. Also, as resonant amplitude variation depicted changes in the conductivity of the growth medium due to bacteria growth, it was selected to detect and monitor bacteria growth.

The temperature variation was recorded as 23.8 $\pm$ 0.4 °C for control i.e., no bacteria, 3 μL, and 9 μL. The environment temperature had no significant impact on the measured results. As the *E. coli* was perfectly confined between the two layers of agar with no air trapped between them, the growth of bacteria based on visual cues indicated bacterial penetration into the agar medium. This was further confirmed by the microscopic images taken at constant time intervals as shown in Fig. 11(a) and (b).

As seen in Fig. 10, a clear distinction between the measured *E. coli* growths can be drawn between 0 μL (control), 3 μL, and 9 μL volume of the bacteria. Maximum amplitude of 0.037 dB was measured for control i.e., with no bacteria and was used as a threshold between the detectable and undetectable regions of bacterial growth. Amplitude variation below the determined threshold value signifies bacterial growth but was undetectable due to know and unknown phenomena such as temperature fluctuations, and changes in the metabolic activity of *E. coli* during lag phase. However, amplitude variation above the threshold indicated bacterial growth, which positively correlated with the microscopic images captured at constant time intervals shown in Fig. 11(a) and (b).

TABLE I
FITTED GOMPERTZ GROWTH MODEL PARAMETERS FOR 3 μL AND 9 μL OF *E. COLI* ON LB AGAR

$$y(t) = A * \exp(-\exp(-K_G * (t - T_i)))$$

E. coli volume	A	K_G	T_i	R^2
3 µL	0.24182	0.08173	19.88572	0.99753
9 µL	0.12456	0.13954	25.59338	0.96736

The rate of change of the measured amplitude correlating to detectable bacterial growth was found by fitting the measured results with the Type I Gompertz growth model. This was obtained by plotting the change in resonant amplitude (Y-axis) and bacterial growth time (X-axis). Type I Gompertz growth model can be described as a sigmoid model often used to describe the growth of animals, plants, and various bacteria and cancer cells [73]. The fitted Gompertz growth curve demonstrated a good agreement with the measured microwave response. The equation governing the Type I Gompertz model is given by (4).

$$y(t) = A * \exp(-\exp(-K_G * (t - T_i))) \quad (4)$$

Where *y(t)* is the expected variation in resonant amplitude as a function of time *t*, *A* represents the upper asymptote (adult value), K_G is the growth rate coefficient (which affects the slope), and T_i represents the time at inflection. The parameter shifts the growth curve horizontally without changing its shape and is, therefore, what has often termed a location parameter (whereas *A* and are shape parameters). Table I presents the calculated Gompertz model parameters for 3 μL and 9 μL of *E. coli*.

As observed from Fig. 11(a) and (b), although no visible bacteria growth was observed up to T = 12 and T = 23 hrs for 3 μL and 9 μL, respectively, the response of the microwave resonator indicated an increase in the variation in conductivity of the growth medium due to bacterial growth. A positive correlation between the measured Δ Resonant amplitude (dB) and the microscopic images successfully established the efficacy of the microstrip resonator sensor for early detection of subsurface bacterial growth prior to any visible bacterial growth.

To demonstrate the strength of the presented method, the operation and results of this work are compared with state-of-the-art publications and are presented in Table II. This work presents a unique approach of a non-contact, label-free microwave biosensor capable of detecting subsurface growth of *E. coli* between two layers of solid LB-agar. The resonant amplitude variation

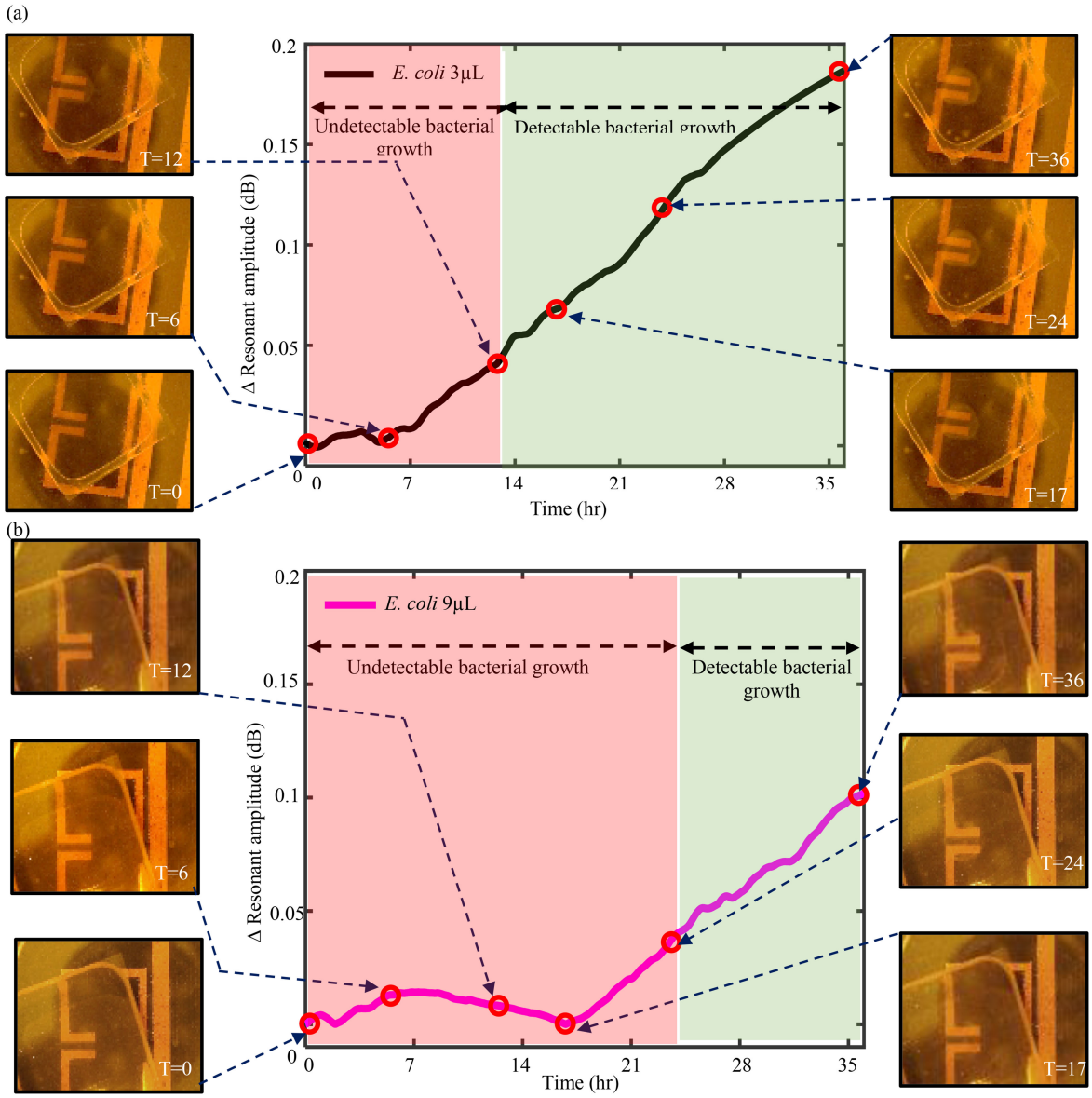

Fig. 11. Measured Δ Amplitude (dB) for (a) 3 μL and (b) 9 μL of *E. coli* and the corresponding *m*icroscope images captured at constant time intervals for 3 μL and 9 μL of *E. coli*.

TABLE II
COMPARISON OF STATE-OF-THE-ART BIOSENSORS TO MONITOR AND DETECT BACTERIAL GROWTH

Microwave sensor type and sensing principle	Method of Detection	Technical Details	Comment
Detection of pathogenic bacteria in aqueous media using interdigitated microwave sensor [49].	Resonant based	-Frequency Range:0.01-15 GHz -Optical density at 550 nm: 1.5	The sensor is in contact with the liquid medium
Real-time, non-contact-based microwave microfluidic ring resonator for *E. coli* detection in liquid LB media [54].	Resonant based	-Operating frequency:2.5 GHz -Maximum sensitivity: 3.4 MHz/log (OD_{600})	The sensor detects *E. coli* growth in liquid medium.
Bacterial growth monitoring on solid LB agar medium using microwave biosensor [60].	Resonant based	-Operating frequencies: 1.95 and 2.11 GHz	The differential sensor detects and monitors surface growth of *E. coli* on solid medium.
Monitoring subsurface bacterial growth between two layers of solid agar medium [This work].	Resonant based	-Operating frequency: 1.76 GHz -Optical density at 600 nm: 1.5	The sensor detects and monitors sub-surface growth of *E. coli.*

was measured for control, 3 μL, and 9 μL *E. coli* volume. Resonant amplitude variation of control corresponding to no growth was measured to be 0.037 dB and was used to distinguish between growth and no-growth of *E. coli*. The rate of change of amplitude, which corresponds to the growth rate of the bacteria was calculated using the Gompertz growth model and was found to be 0.08173 dB/hr. and 0.13954 dB/hr. for 3 μL and 9 μL of *E. coli*, respectively. The performance of the microwave sensor to accurately monitor and detect the growth of bacteria was validated through measurements and microscope images.

V. Conclusion

In this work, a non-contact, label-free microwave-based biosensor capable of detecting and monitoring subsurface growth of *E. coli* between two layers of LB-agar is presented. The sensing apparatus consists of a one-port microstrip ring resonator operating at 1.76 GHz. Bacterial metabolism is accompanied by variations in the conductivity of the growth medium. Resonant amplitude is sensitive to conductivity or loss tangent variations as evident from this study further suggest that resonant amplitude can be used as a preferred index over resonant frequency to monitor bacterial growth. The fitting of bacterial growth measurement to the Gompertz growth model shows the potential of the currently used sensing tool for bacterial monitoring. Also, this study opens a wide arena of microwave applications in clinical research for early detection of biofilm-forming bacterial infections, which has implications for the medical and food processing industries.

Acknowledgment

The authors would like to thank the Syilx Okanagan Nation for the use of their unceded territory, the land on which the research was conducted. We would like to acknowledge Professor Deborah June Roberts (Biological Solutions Laboratory, UBC Okanagan) for providing facilities to conduct microbiology experiments. We would also like to thank Dr. Tyler J. Donner for providing bacterial cultures.

References

[1] N. Zhu *et al.*, "A novel coronavirus from patients with pneumonia in China, 2019," *New England J. Med.*, vol. 382, no. 8, pp. 727–733, Feb. 2020.

[2] E. K. Stevenson, A. R. Rubenstein, G. T. Radin, R. S. Wiener, and A. J. Walkey, "Two decades of mortality trends among patients with severe sepsis: A comparative meta-analysis*," *Crit. Care Med.*, vol. 42, no. 3, pp. 625–631, Mar. 2014.

[3] H.-U. Meier-Kriesche, A. O. Ojo, J. A. Hanson, and B. Kaplan, "Exponentially increased risk of infectious death in older renal transplant recipients," *Kidney Int.,* vol. 59, no. 4, pp. 1539–1543, Apr. 2001.

[4] L. van der Hoek *et al.*, "Identification of a new human coronavirus," *Nat. Med.*, vol. 10, no. 4, pp. 368–373, Apr. 2004.

[5] J. M. O'Brien, N. A. Ali, S. K. Aberegg, and E. Abraham, "Sepsis," *Amer. J. Med.*, vol. 120, no. 12, pp. 1012–1022, Dec. 2007.

[6] M. A. Nazir, "Prevalence of periodontal disease, its association with systemic diseases and prevention," *Int. J. Health Sci. (Qassim)*, vol. 11, no. 2, pp. 72–80, 2017.

[7] E. Livingston, K. Bucher, and A. Rekito, "Coronavirus disease 2019 and influenza 2019-2020," *JAMA*, vol. 323, no. 12, Mar. 2020, Art. no. 1122.

[8] M. Hassan, E. Gonzalez, V. Hitchins, and I. Ilev, "Detecting bacteria contamination on medical device surfaces using an integrated fiber-optic mid-infrared spectroscopy sensing method," *Sensors Actuators B Chem.*, vol. 231, pp. 646–654, Aug. 2016.

[9] T. Javanbakht, B. Ghane-Motlagh, and M. Sawan, "Comparative study of antibiofilm activity and physicochemical properties of microelectrode arrays," *Microelectron. Eng.*, vol. 229, Mar. 2020, Art. no. 111305.

[10] M. A. A. Grant, B. Wacław, R. J. Allen, and P. Cicuta, "The role of mechanical forces in the planar-to-bulk transition in growing Escherichia coli microcolonies," *J. Roy. Soc. Interface*, vol. 11, no. 97, Aug. 2014, Art. no. 20140400.

[11] D. Lebeaux, J.-M. Ghigo, and C. Beloin, "Biofilm-related infections: Bridging the gap between clinical management and fundamental aspects of recalcitrance toward antibiotics," *Microbiol. Mol. Biol. Rev.*, vol. 78, no. 3, pp. 510–543, Sep. 2014.

[12] Z. Khatoon, C. D. McTiernan, E. J. Suuronen, T.-F. Mah, and E. I. Alarcon, "Bacterial biofilm formation on implantable devices and approaches to its treatment and prevention," *Heliyon*, vol. 4, no. 12, Dec. 2018, Art. no. e01067.

[13] S. S. Magill *et al.*, "Multistate point-prevalence survey of health care–associated infections," *New England J. Med.*, vol. 370, no. 13, pp. 1198–1208, Mar. 2014.

[14] R. J. Allen and B. Waclaw, "Bacterial growth: A statistical physicist's guide," *Rep. Prog. Phys.*, vol. 82, no. 1, Jan. 2019, Art. no. 016601.

[15] R. J. Allen and B. Waclaw, "Europe PMC funders group bacterial growth: A statistical physicist's guide," *Rep. Prog. Phys.*, vol. 82, no. 1, pp. 1–55, 2019.

[16] F. Si, B. Li, W. Margolin, and S. X. Sun, "Bacterial growth and form under mechanical compression," *Sci. Rep.*, vol. 5, no. 1, Sep. 2015, Art. no. 11367.

[17] P. L. Young and L. A. Olse, *The Healthcare Imperative*. Washington, D.C., USA: National Academies Press, 2010.

[18] S. A. Barghouthi, "A universal method for the identification of bacteria based on general PCR primers," *Indian J. Microbiol.*, vol. 51, no. 4, pp. 430–444, Oct. 2011.

[19] J.-C. Lagier, S. Edouard, I. Pagnier, O. Mediannikov, M. Drancourt, and D. Raoult, "Current and past strategies for bacterial culture in clinical microbiology," *Clin. Microbiol. Rev.*, vol. 28, no. 1, pp. 208–236, Jan. 2015.

[20] R. Franco-Duarte *et al.*, "Advances in chemical and biological methods to identify microorganisms—From past to present," *Microorganisms*, vol. 7, no. 5, pp. 130–162, May 2019.

[21] P. Cheng *et al.*, "A novel regeneration-free E. coli O157:H7 amperometric immunosensor based on functionalised four-layer magnetic nanoparticles," *Sensors Actuators B Chem.,* vol. 204, pp. 561–567, Dec. 2014.

[22] Y. Wang, Z. Ye, C. Si, and Y. Ying, "Monitoring of Escherichia coli O157:H7 in food samples using lectin based surface plasmon resonance biosensor," *Food Chem.*, vol. 136, no. 3/4, pp. 1303–1308, Feb. 2013.

[23] A.-R. H. A.-A. Hassan, A. de la Escosura-Muñiz, and A. Merkoçi, "Highly sensitive and rapid determination of escherichia coli O157:H7 in minced beef and water using electrocatalytic gold nanoparticle tags," *Biosens. Bioelectron.*, vol. 67, pp. 511–515, May 2015.

[24] M. Pohanka, "The piezoelectric biosensors: Principles and applications, a review," *Int. J. Electrochem. Sci.*, vol. 12, pp. 496–506, Jan. 2017.

[25] L. Yao *et al.*, "CMOS conductometric system for growth monitoring and sensing of bacteria," *IEEE Trans. Biomed. Circuits Syst.*, vol. 5, no. 3, pp. 223–230, Jun. 2011.

[26] M. Salami, A. Mhs, M. Sawan, and A. Nsk, "Biosensors & bioelectronics biofet-based integrated platform for accurate and rapid detection of E. coli bacteria: A review," *J. Biosens. Bioelectron.*, vol. 10, no. 1, pp. 1–11, 2019.

[27] G. Nabovati, E. Ghafar-Zadeh, and M. Sawan, "A 64 pixel ISFET-based biosensor for extracellular pH gradient monitoring," in *Proc. IEEE Int. Symp. Circuits Syst.*, 2015, pp. 1762–1765.

[28] E. Ghafar-Zadeh, M. Sawan, V. P. Chodavarapu, and T. Hosseini-Nia, "Bacteria growth monitoring through a differential CMOS capacitive sensor," *IEEE Trans. Biomed. Circuits Syst.*, vol. 4, no. 4, pp. 232–238, Aug. 2010.

[29] G. Nabovati, E. Ghafar-Zadeh, A. Letourneau, and M. Sawan, "Towards high throughput cell growth screening: A new CMOS 8 $\times$ 8 biosensor array for life science applications," *IEEE Trans. Biomed. Circuits Syst.*, vol. 11, no. 2, pp. 380–391, Apr. 2017.

[30] B. Wiltshire, K. Mirshahidi, K. Golovin, and M. H. Zarifi, "Robust and sensitive frost and ice detection via planar microwave resonator sensor," *Sensors Actuators B Chem.*, vol. 301, no. May, Dec. 2019, Art. no. 126881.

[31] N. M. C. Hurtado, M. H. Zarifi, M. Daneshmand, and J. A. Llobet, "Flexible microdisplacement sensor for wearable/implantable biomedical applications," *IEEE Sens. J.*, vol. 17, no. 12, pp. 3873–3883, Jun. 2017.

[32] K. Saeed, R. D. Pollard, and I. C. Hunter, "Substrate integrated waveguide cavity resonators for complex permittivity characterization of materials," *IEEE Trans. Microw. Theory Tech.*, vol. 56, no. 10, pp. 2340–2347, Oct. 2008.

[33] B. D. Wiltshire, S. Mohammadi, and M. H. Zarifi, "Integrating 3D printed microfluidic channels with planar resonator sensors for low cost and sensitive liquid detection," in *Proc. 18th Int. Symp. Antenna Technol. Appl. Electromagn.*, 2018, pp. 1–2.
[34] M. H. Zarifi and M. Daneshmand, "High-Resolution RFID liquid sensing using a chipless tag," *IEEE Microw. Wireless Compon. Lett.*, vol. 27, no. 3, pp. 311–313, Mar. 2017.
[35] B. D. Wiltshire and M. H. Zarifi, "3-D printing microfluidic channels with embedded planar microwave resonators for RFID and liquid detection," *IEEE Microw. Wireless Compon. Lett.*, vol. 29, no. 1, pp. 65–67, Jan. 2019.
[36] M. A. Rafi, B. D. Wiltshire, and M. H. Zarifi, "Wideband tunable modified split ring resonator structure using liquid metal and 3-D printing," *IEEE Microw. Wireless Compon. Lett.*, vol. 30, no. 5, pp. 469–472, May 2020.
[37] M. A. Suster, D. Maji, N. Vitale, U. Gurkan, and P. Mohseni, "An RF/microwave microfluidic sensor for miniaturized dielectric spectroscopy based on sensor transmission characteristics," in *Proc. IEEE Sens.*, 2015, pp. 1–4.
[38] M. A. Suster and P. Mohseni, "An RF/microwave microfluidic sensor based on a center-gapped microstrip line for miniaturized dielectric spectroscopy," in *Proc. IEEE MTT-S Int. Microw. Symp. Digit.*, 2013, pp. 1–3.
[39] D. Maji *et al.*, "A novel, point-of-care, whole-blood assay utilizing dielectric spectroscopy is sensitive to coagulation factor replacement therapy in haemophilia a patients," *Haemophilia*, vol. 25, no. 5, pp. 885–892, Sep. 2019.
[40] M. A. Suster, B. Blackburn, U. Gurkan, and P. Mohseni, "An RF/microwave microfluidic sensor based on a 3D capacitive structure with a floating electrode for miniaturized dielectric spectroscopy," in *Proc. IEEE Sens.*, 2014, pp. 1784–1787.
[41] S. Afshar, A. Fazelkhah, E. Salimi, M. Butler, D. J. Thomson, and G. E. Bridges, "Dielectric properties of single cells subjected to heat shock using DEP cytometry," *IEEE Trans. Microw. Theory Tech.*, vol. 66, no. 12, pp. 5933–5940, Dec. 2018.
[42] L. Wang, "Microwave sensors for breast cancer detection," *Sensors*, vol. 18, no. 2, pp. 655–672, Feb. 2018.
[43] P. Velez, J. Munoz-Enano, K. Grenier, J. Mata-Contreras, D. Dubuc, and F. Martin, "Split ring resonator-based microwave fluidic sensors for electrolyte concentration measurements," *IEEE Sens. J.*, vol. 19, no. 7, pp. 2562–2569, Apr. 2019.
[44] A. Ebrahimi, J. Scott, and K. Ghorbani, "Microwave reflective biosensor for glucose level detection in aqueous solutions," *Sensors Actuators A Phys.,* vol. 301, Jan. 2020, Art. no. 111662.
[45] A. Ebrahimi, J. Scott, and K. Ghorbani, "Highly sensitive microwave-based biosensor for electrolytic level measurement in water," in *Proc. IEEE Asia-Pacific Microw. Conf.*, 2019, pp. 759–761.
[46] A. Ebrahimi, W. Withayachumnankul, S. F. Al-Sarawi, and D. Abbott, "Microwave microfluidic sensor for determination of glucose concentration in water," in *Proc. IEEE 15th Mediterranean Microw. Symp.*, 2015, pp. 1–3.
[47] S. Mohammadi *et al.*, "Gold coplanar waveguide resonator integrated with a microfluidic channel for aqueous dielectric detection," *IEEE Sens. J.*, vol. 20, no. 17, pp. 9825–9833, Sep. 2020.
[48] S. Mohammadi, A. V. Nadaraja, D. J. Roberts, and M. H. Zarifi, "Real-time and hazard-free water quality monitoring based on microwave planar resonator sensor," *Sensors Actuators A Phys.,* vol. 303, Nov. 2019, Art. no. 111663.
[49] I. Nakouti, O. Korostynska, A. Mason, and A. I. Al-Shamma'a, "Detection of pathogenic bacteria in aqueous media: Assessing the potential of real-time electromagnetic wave sensing," in *Proc. Int. Conf. Sens. Technol.*, 2014, pp. 140–145.
[50] G. A. Ferrier, S. F. Romanuik, D. J. Thomson, G. E. Bridges, and M. R. Freeman, "A microwave interferometric system for simultaneous actuation and detection of single biological cells," *Lab Chip*, vol. 9, no. 23, 2009, Art. no. 3406.
[51] P. Velez, K. Grenier, J. Mata-Contreras, D. Dubuc, and F. Martin, "Highly-sensitive microwave sensors based on open complementary split ring resonators (OCSRRs) for dielectric characterization and solute concentration measurement in liquids," *IEEE Access*, vol. 6, pp. 48324–48338, 2018.
[52] G. Bridges, T. Cabel, S. Afshar, E. Salimi, D. Thomson, and M. Butler, "Microwave near-field detection of single biological cells and nanoparticles," in *Proc. 18th Int. Symp. Antenna Technol. Appl. Electromagn.*, 2018, pp. 1–2.
[53] S. Mohammadi, R. Narang, M. M. Ashani, H. Sadabadi, A. Sanati-Nezhad, and M. H. Zarifi, "Real-time monitoring of Escherichia coli concentration with planar microwave resonator sensor," *Microw. Opt. Technol. Lett.*, vol. 61, no. 11, pp. 2534–2539, Nov. 2019.
[54] R. Narang *et al.*, "Sensitive, real-time and non-intrusive detection of concentration and growth of pathogenic bacteria using microfluidic-microwave ring resonator biosensor," *Sci. Rep.*, vol. 8, no. 1, Dec. 2018, Art. no. 15807.
[55] I. Piekarz *et al.*, "A microwave matrix sensor for multipoint label-free escherichia coli detection," *Biosens. Bioelectron.*, vol. 147, Jan. 2020, Art. no. 111784.
[56] A. Sanchis *et al.*, "Dielectric characterization of bacterial cells using dielectrophoresis," *Bioelectromagnetics*, vol. 28, no. 5, pp. 393–401, Jul. 2007.
[57] W. Bai, K. S. Zhao, and K. Asami, "Dielectric properties of E. coli cell as simulated by the three-shell spheroidal model," *Biophys. Chem.*, vol. 122, no. 2, pp. 136–142, Jul. 2006.
[58] B. Zavizion, Z. Zhao, A. Nittayajarn, and R. J. Rieder, "Rapid microbiological testing: Monitoring the development of bacterial stress," *PLoS One*, vol. 5, no. 10, Oct. 2010, Art. no. e13374.
[59] M. Schaechter, "A brief history of bacterial growth physiology," *Front. Microbiol.*, vol. 6, pp. 1–5, Apr. 2015.
[60] S. Mohammadi, A. V. Nadaraja, K. Luckasavitch, M. C. Jain, D. J. Roberts, and M. H. Zarifi, "A label-free, non-intrusive, and rapid monitoring of bacterial growth on solid medium using microwave biosensor," *IEEE Trans. Biomed. Circuits Syst.*, vol. 14, no. 1, pp. 2–11, Feb. 2020.
[61] M. C. Jain, A. V. Nadaraja, B. M. Vizcaino, D. J. Roberts, and M. H. Zarifi, "Differential microwave resonator sensor reveals glucose-dependent growth profile of E. coli on solid agar," *IEEE Microw. Wireless Compon. Lett.*, vol. 30, no. 5, pp. 531–534, May 2020.
[62] L. L. Hause, R. A. Komorowski, and F. Gayon, "Electrode and electrolyte impedance in the detection of bacterial growth," *IEEE Trans. Biomed. Eng.*, vol. BME-28, no. 5, pp. 403–410, May 1981.
[63] J. B. Allison, J. A. Anderson, and W. H. Cole, "The method of electrical conductivity in studies on bacterial metabolism.," *J. Bacteriol.*, vol. 36, no. 6, pp. 571–586, Dec. 1938.
[64] R. Firstenberg-Eden and J. Zindulis, "Electrochemical changes in media due to microbial," *J. Microbiol. Methods*, vol. 2, no. 2, pp. 103–115, Mar. 1984.
[65] K. Krishnamurti and S. R. Kate, "Changes in electrical conductivity during bacterial growth," *Nature*, vol. 168, no. 4265, pp. 170–170, Jul. 1951.
[66] R. J. King, "Microwave reflection resonator sensors," US Patent 5334941, Aug. 2, 1994.
[67] J. Garrett and E. Fear, "Average dielectric property analysis of complex breast tissue with microwave transmission measurements," *Sensors*, vol. 15, no. 1, pp. 1199–1216, Jan. 2015.
[68] J. Muñoz-Enano, P. Vélez, M. Gil, and F. Martín, "Planar microwave resonant sensors: A review and recent developments," *Appl. Sci.*, vol. 10, no. 7, Apr. 2020, Art. no. 2615.
[69] D. M. Pozar, *Microwave Engineering*. 3rd ed., Hoboken, NJ, USA: Wiley, 2005.
[70] P. Jurtshuk, "Bacterial Metabolism," in *Medical Microbiology*, 4th ed., Samuel Baron, Ed. Galveston: University of Texas Medical Branch at Galveston, 1996, pp. 32–48.
[71] S. Jankovic, M. Milosev, and M. Novakovic, "The effects of microwave radiation on microbial cultures," *Hosp. Pharmacol. - Int. Multidiscip. J.*, vol. 1, no. 2, pp. 102–108, 2014.
[72] Rogers Corporation, "Technisches datenblatt RT/duroid 5880," Advanced Connectivity Solutions, Chandler, Arizona, USA, 2017. Accessed: Sep. 19, 2020. [Online]. Available: https://rogerscorp.com/-/media/project/rogerscorp/documents/advanced-connectivity-solutions/english/data-sheets/rt-duroid-5870---5880-data-sheet.pdf
[73] K. M. C. Tjørve and E. Tjørve, "The use of gompertz models in growth analyses, and new Gompertz-model approach: An addition to the unified-richards family," *PLoS One*, vol. 12, no. 6, Jun. 2017, Art. no. e0178691.

Mandeep Chhajer Jain (Student Member, IEEE) received the B.Sc. degree in electronics and communication engineering from Jawaharlal Nehru Technological University, Hyderabad, India, in 2017. He is currently working toward the M.A.Sc degree in electrical engineering with the University of British Columbia, Vancouver, BC, Canada, and is working on microwave sensors for biomedical application. From 2016 to 2018, he was first an Intern with Amazon Development Center Ltd as a DevOps Engineer and then a Full-time Employee. He holds a Certificate of Achievement for his oral presentation in the 5th Annual Engineering Graduate Symposium (AEGS 2019) held at the University of British Columbia Okanagan, Kelowna, BC, Canada.

Anupama Vijaya Nadaraja received the B.Sc. degree in biotechnology from the University of Kerala, Thiruvananthapuram, India, the M.Sc. degree in biotechnology from Manonmaniam Sundaranar University, Tirunelveli, India, and the Ph.D. degree in biotechnology from the Environmental Technology Division, Council of Scientific and Industrial Research National Institute for Interdisciplinary Science and Technology, Thiruvananthapuram, India, in 2015. She is currently a Postdoctoral Fellow with the School of Engineering, The University of British Columbia (UBC) Okanagan, Kelowna, BC, Canada. Before joining UBC, she was a Postdoctoral Fellow with the Department of Biotechnology, University of Kerala from 2016 to 2017. She has authored or coauthored more than 18 publications in peer-reviewed journals, seven conference proceedings and one patent. Her current research interests include exploring the applications of microwave sensors on biological systems and process development for water or wastewater treatment.

Sevda Mohammadi (Student Member, IEEE) received the B.Sc. degree in electrical engineering from Urmia University, Urmia, Iran, and the M.Sc. degree in electrical engineering from the K.N. Toosi University of Technology, Tehran, Iran, in 2013 and 2015, respectively. She is currently working toward the Ph.D. degree in microwave sensor structures and analog or mixed-signal integrated circuits with the University of British Columbia, Vancouver, BC, Canada. Since 2015, she has been actively involved in industry supported R&D projects and has contributed to the development of various HDL-based digital modules or interfacing circuits. She was the recipient of the first place in Iranian Micro-electronics Olympiad Competition in 2017.

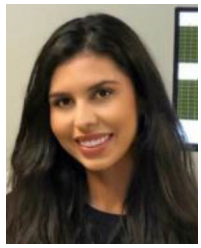

Bianca Marjan Vizcaino is currently a third year student working toward the B.Sc. degree in biology and psychology with the University of British Columbia Okanagan, Kelowna, BC, Canada. Her research interests include gaining insight into interdisciplinary research and combining her diverse skills to explore electrical and biomedical engineering. She is passionate about learning how various technological advancements can transform the healthcare industry.

Mohammad Hossein Zarifi (Senior Member, IEEE) received the B.Sc., M.Sc., and Ph.D. degrees in electrical and computer engineering from the University of Tabriz, Tabriz, Iran, in 2004, 2006, and 2009, respectively. He is currently an Assistant Professor with the School of Engineering, The University of British Columbia, Kelowna, BC, Canada and the Director with Okanagan Microelectronics and Gigahertz Laboratory, Kelowna, Canada. From 2013 to 2017, he was a Postdoctoral Fellow with the University of Alberta, Edmonton, AB, Canada. He has authored or coauthored more than 75 papers in peer-reviewed journal and conference proceedings and has five issued or pending patents. His research interests include the design of high-speed and low-power analog circuits, analog-to-digital converters for biomedical and communication applications, microwave planar structures for sensing applications, and investigating the new emerging technologies for the state-of-the-art sensors, with focus on microwave resonators. He was the recipient of the CMC-NRC First Place Award on industrial collaboration for the innovative microwave sensors in Canada in 2015. He is a Senior Member of the IEEE Solid-State Circuits Society, the IEEE Circuits and Systems Society and was a reviewer for different journals and conferences.